Verification of Knoop indenters with a Vickers-addressed optical system

Original
Verification of Knoop indenters with a Vickers-addressed optical system / Prato, Andrea; Origlia, Claudio; Germak, Alessandro. - In: MEASUREMENT. - ISSN 0263-2241. - 163:(2020), p. art. no. 107928. [10.1016/j.measurement.2020.107928]

Publisher:
Elsevier

Published
DOI:10.1016/j.measurement.2020.107928

Verification of Knoop indenters with a Vickers-addressed optical system

Andrea Prato[1]*, Claudio Origlia*[1] *and Alessandro Germak*[1]

[1] *INRiM - Istituto Nazionale di Ricerca Metrologica, 10135 Torino, Italy*

Corresponding author e-mail: *a.prato@inrim.it*

Abbreviated title: Knoop indenters verification with optical system

Abstract

ISO 4545-2 and 4545-3 of Knoop hardness tests require the geometrical verification of the indenters. INRiM hardness laboratory, in cooperation with Galileo-LTF®, has developed the Gal-Indent optical measuring system for the verification of Vickers indenters. This system can measure the vertex angles between two opposite faces, the quadrilateral base angles and the pyramid axis tilt angle. Using these measured quantities as inputs of a suitable geometrical model, the angles between the opposite edges at the vertex of Knoop indenters, nominally 172.5° and 130°, and the angle between the pyramid and indenter holder axes can be verified with an expanded uncertainty of 0.05°. Comparison of experimental measurements performed on three different Knoop indenters, previously verified by an accredited laboratory, shows compatible results. The proposed geometrical model could be easily implemented by laboratories that adopt similar measuring systems addressed for the verification of Vickers indenters without any modification of the experimental apparatus.

Keywords: Hardness, Knoop indenter, Geometrical model, Gal-indent optical system.

1. Introduction

Knoop indenter is a pyramidal diamond with a robic quadrilateral base that produces an elongated indent. The angles between the opposite edges at the vertex of the diamond pyramid of the indenter, α and β, are 172.5° and 130°, respectively, and the ratio between long and short diagonals is approximately 7.11 to 1 (Fig. 1). This entails that the angles of the rhombic base, φ_i and τ_i (i=1,2), are approximately 164° and 16°, respectively, and that the angles between the two opposite faces of the vertex θ are approximately 129.57°.

These characteristics make Knoop hardness ideal for testing surface defects, brittle materials and small specimens, including thin metal films [1]. Moreover, due to the sensitivity of Knoop hardness to the indenter orientation, it is useful to evaluate the anisotropy of materials [2]. The influence of indenter characteristics on hardness measurements is largely reported in literature in particular for Vickers and Rockwell hardness. By performing the analysis of variances on a large set of Vickers and Rockwell tests, it was found that the geometry of the indenters was statistically significant in most of the cases [3] producing a relevant uncertainty contribution [4]. In Rockwell hardness, besides tip radius and cone angle, this can also be due to roughness, indenter deformations under load [5] or to the soldering of the diamond cone into the holder [6]. In addition, it was found that increasing the cone angle and the tip radius of the indenter entails an increase in Rockwell hardness value [7]. In Vickers hardness, on the contrary, it was found that an indenter with a larger angle, although within the limits allowed by the ISO standard, entails a wider indentation, thus a decrease in hardness value [8], which might exceed permissible values [9]. However for Knoop hardness, few studies on the influence of the indenter geometry are found. One showed that small geometric imperfections of the indeters have a negligible influence on the contact area but a noticeable influence on the force–depth response [10]. Others showed that the influence of indenter geometry on hardness may not be negligible when testing enamels [11] and cobalt-based alloys [12]. Furthermore, in depth-sensing indentation, it was shown that the geometry of Knoop indenter affects the evaluation Young’s modulus of the indented material [13], while, in nanoindentation, non-geometrically perfect Knoop indenters provide accurate results even at the very low loads at which a nanoindenter operates [14].

ISO 4545-2 and 4545-3 [15,16] specify the requirements of the indenters with different tolerances. The second is more restrictive since it refers to the calibration of reference blocks. The tolerance for the angle of

172.5° is ±0.1° in both documents, whereas for the angle of 130° the tolerance is ±1° and ±0.1°, respectively. Furthermore, the angle δ between the axis of the diamond pyramid and the axis of the indenter holder (normal to the seating surface), named tilt angle, shall not exceed 0.5° and 0.3°, respectively. The four faces of the diamond pyramid shall also be polished and free from surface defects and the indenter constant $c=\tan(\beta/2)/(2\tan(\alpha/2))$ shall be within 1,0 % of the ideal value 0.07028, i.e. $0.06958 \leqslant c \leqslant 0.07098$. In addition, the device used for the verification shall have a maximum expanded uncertainty of 0.07°.

At present, verification of Knoop hardness is performed by few manufacturers and laboratories that own specific instrumentation addressed for the scope. Conversely, verification of squared-based Vickers indenters, based on the measurement of the angles between the opposite faces of the vertex, the squareness of the quadrilateral base angles and the angle between the axis of the diamond pyramid and the axis of the indenter holder, can be performed by a larger number of calibration laboratories and industries with dedicated systems. Given the similar geometry of the two indenters, in this paper it is investigated the possibility to use Vickers-addressed systems for the verification of Knoop indenters by implementing a simple geometrical model, in order to extend the measurement capability of these laboratories without changing the experimental apparatus or developing new ones.

Verification of Vickers indenters is usually performed with optical measuring systems using scanning interferometry [17], microscopes [18] or scanning confocal probes [19]. INRiM hardness laboratory, in cooperation with Galileo-LTF® [20,21], has developed a specific optical measuring system (commercialized by the Galileo-LTF® as Gal-Indent) for the verification of the geometry of Vickers indenters [22]. This system is able to directly measure the main geometrical parameters of Vickers indenters required by the standard, i.e. the two vertex angles between two opposite faces, the four angles of the square base, and the angle between the axis of the diamond pyramid and the axis of the indenter holder, with an expanded uncertainty of 0.05°. By measuring these quantities for Knoop indenters and with a suitable geometrical model, the possibility to evaluate their geometrical parameters required by the relevant Standards is investigated. This paper deals with a brief description of the Gal-Indent optical system (Section 2), the geometrical model (Section 3) and a comparison of experimental results among three different Knoop indenters with values obtained by a German accredited laboratory to validate the proposed method (Section 4).

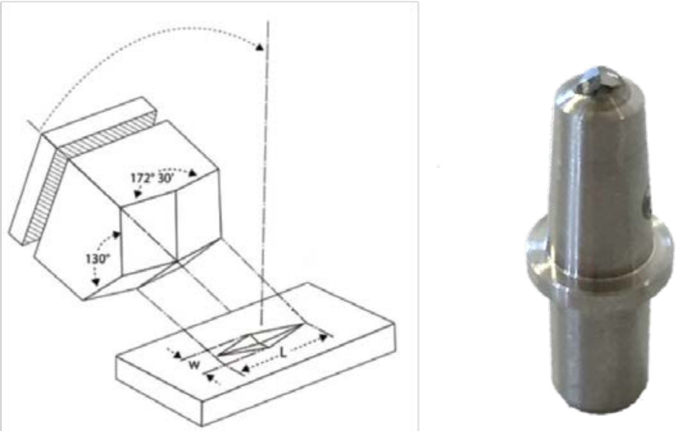

Fig. 1. Schematic draw (left) [23] and picture (right) of a Knoop indenter.

2. The Gal-Indent optical system

In INRiM hardness laboratory a specific measuring system, commercialized by Galileo-LTF® as Gal-Indent optical system (Fig. 2), was developed and is currently used for the verification of Vickers indenters. The system is also adopted by different National Metrological Institutes (NMIs) and calibration laboratories around the world. It is able to measure the vertex angle of the indenter between two opposite faces, and the quadrilateral base angles by means of two angular encoders [24]. The optical system is based on Mirau interferometry. A green laser beam with a wavelength of 546 nm, emitted by a light source, is divided in two beams: the first reaches the observer through the eyepiece and the second strikes the surface of the indenter and is reflected back creating an interference pattern. Through a mechanical system, the indenter is simultaneously rotated around the indenter-holder axis and around the axis parallel to the plane of the microscope lens passing through the diamond pyramid vertex until the number of interference fringes is minimized, thus obtaining a lateral indenter face parallel to the microscope lens. These two rotations are measured by means of two angular encoders. The first rotation, around the indenter-holder axis, represents the measurement of quadrilateral base angles. The second rotation around the axis parallel to the plane of the lens represents the measurement of the supplementary angles of each lateral face from which the angles between two opposite faces and the angle between the axis of the diamond pyramid and the axis of the indenter holder are obtained [25], as required for the verification of Vickers indenters. Using these measurements as input of a suitable geometrical model, presented in the following Section, the possibility to evaluate the geometrical parameters of Knoop indenters is investigated.

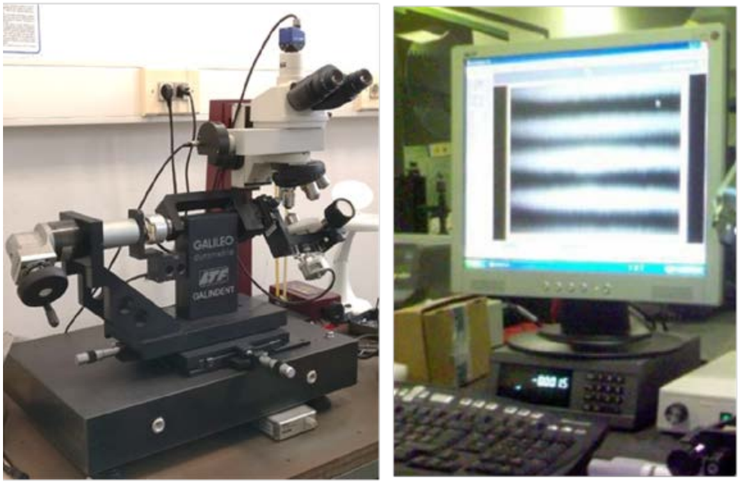

Fig. 2. The Galileo-LTF® Gal-Indent optical system.

3. The geometrical model

3.1 Evaluation of the tilt angle

The geometry of an ideal Knoop indenter, i.e. an indenter with four generic faces (A, B, C, D), with angles between the opposite edges at the vertex of the diamond pyramid α and β equal to 172.5° and 130°, respectively, with angles θ between two opposite faces equal to 129.57°, and with a tilt angle δ equal to 0°, is schematically depicted in Fig. 3. *xyz* and *x'y'z'* coordinate systems correspond, respectively, to the diagonals of the Knoop indenter rhombic base, and to the optical reference system that is perpendicular to the perimeter of two opposite faces. Therefore, the angle between *x*- and *y*-axis is nominally 90°, whereas the angle σ_{AB} between *x'*- and *y'*-axis is nominally 164°. For each *j*-th face (*j*=A, B, C, D), the intersection between an optical reference axis (*x'*- or *y'*-axis) and the base perimeter is identified by point H_j, whereas the intersection with *x*- and *y*-axis are identified by points S_j and P_j, respectively (thus $S_A \equiv S_D$, $S_B \equiv S_C$, $P_A \equiv P_B$, $P_C \equiv P_D$). The pyramid vertex V is arbitrally placed on z=1. A cross-section of an ideal Knoop indenter along *x'z'* optical system plane is also shown in Fig. 4. The quadrilateral base angles φ_i and τ_i (i=1,2), nominally 164° and 16°, respectively, and the supplementary angles of each *j*-th lateral face (A, B, C, D) along *x*′ and *y*′-axis, ω_j, nominally (180°-129.57°)/2≈25.22°, are measured by means of the optical system previously described.

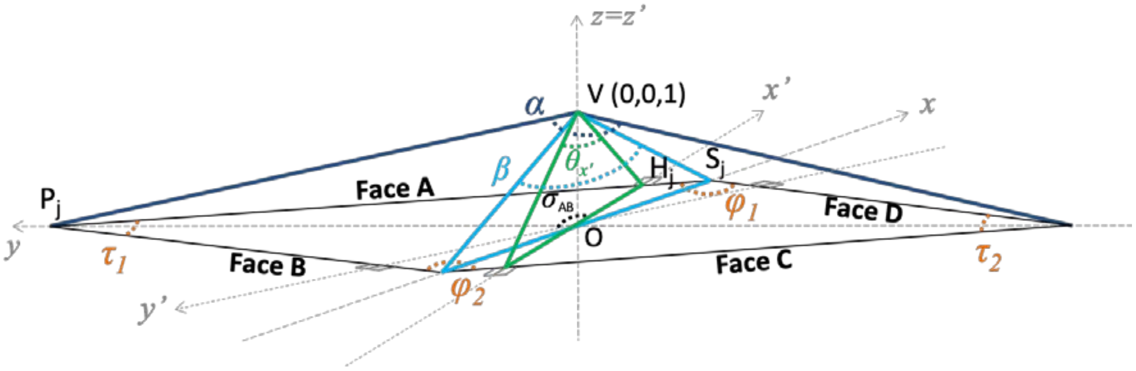

Fig. 3. 3-D schematic representation of an ideal Knoop indenter rhombic-based pyramid.

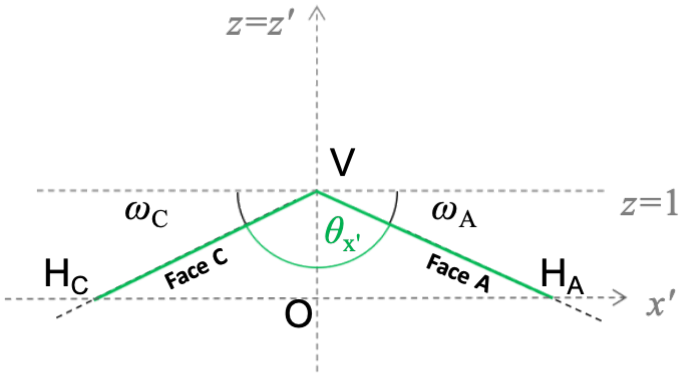

Fig. 4. Cross-section of an ideal Knoop indenter along *x*′*z*′ optical reference system plane.

However, in real Knoop indenters, the tilt angle δ between the axis of the diamond pyramid $\mathbf{v}=\overrightarrow{OV}=(v_x,v_y,v_z)$ and the axis of the indenter holder angle (*z*′-axis) is not exactly 0°, thus an angle γ between the projection of the pyramid vertex on $z=0$ plane and *x*′-axis appears, as shown in Fig. 5.

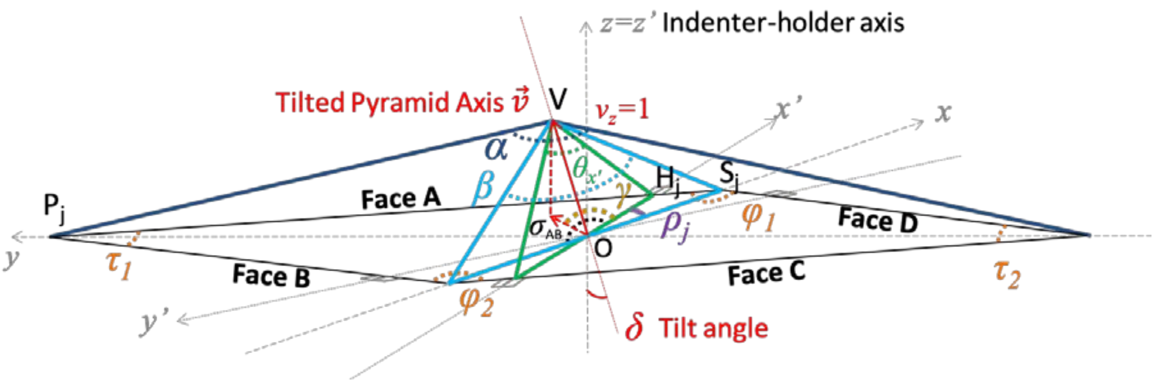

Fig. 5. 3-D schematic representation of a real Knoop indenter rhombic-based pyramid.

From quadrilateral base angles measurements φ_i and τ_i (i=1,2), in order to take into account possible asymmetries of the rhombic-base, the mean angle $\rho_j = \widehat{H_j O S_j}$ between xy and $x'y'$ reference systems (e.g., in Fig. 5 for face A between x'- and x-axis), for each j-th indenter face, can be evaluated according to

$$\rho_j = \frac{\left(90 - \frac{\varphi_j}{2}\right) + \frac{\tau_j}{2}}{2} \tag{1}$$

where $\varphi_A=\varphi_D=\varphi_1$, $\varphi_B=\varphi_C=\varphi_2$, $\tau_A=\tau_B=\tau_1$, $\tau_C=\tau_D=\tau_2$.

In this way, considering the mean value $\rho = \sum_{j=1}^{4} \rho_j/4$ among the four faces, the angle σ_{AB} between x'- and y'-axis can be obtained according to Eq. (2).

$$\sigma_{AB} = 180 - 2\rho \tag{2}$$

From the measurement of the supplementary angles ω_j of each j-th lateral face, the two vertex angles $\theta_{x'}$ and $\theta_{y'}$ and the pyramid tilt angles $\delta_{x'}$ and $\delta_{y'}$, along x'- and y'- axis, can be calculated according to Eqs. (3) and (4), respectively. In Fig. 6, the cross-section of a real Knoop indenter through $x'z'$ plane with vertex angle $\theta_{x'}$ and pyramid tilt angle $\delta_{x'}$ is depicted.

$$\theta_{x'} = 180 - (\omega_A + \omega_C); \qquad \theta_{y'} = 180 - (\omega_B + \omega_D) \tag{3}$$

$$\delta_{x'} = \frac{\omega_A - \omega_C}{2}; \quad \delta_{y'} = \frac{\omega_B - \omega_D}{2} \tag{4}$$

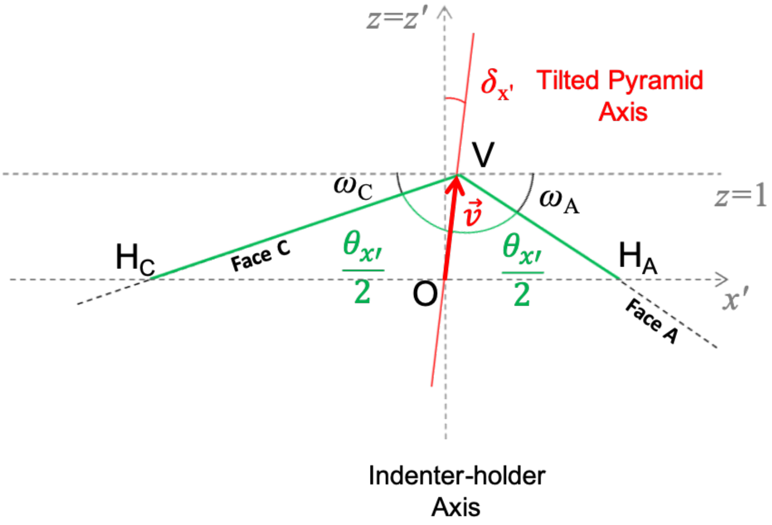

Fig. 6. Cross-section of a real Knoop indenter along *x'z'* optical reference system plane.

By projecting the pyramid tilted axis vector **v** along non-orthogonal *x'z'* and *y'z'* planes, according to Fig. 7 and Fig. 8, Eq. (5) is derived. Successively, implementing the equations of non-orthogonal systems (Fig. 9) and using Eq. (5), Eqs. (6)-(8) and Eqs. (9)-(10) can be derived.

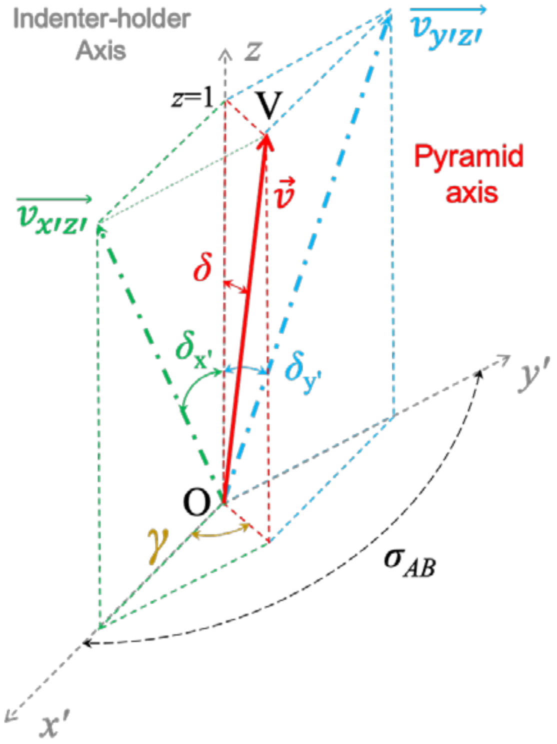

Fig. 7. Projection of Knoop indenter axis **v** along *x'*- and *y'*- axis.

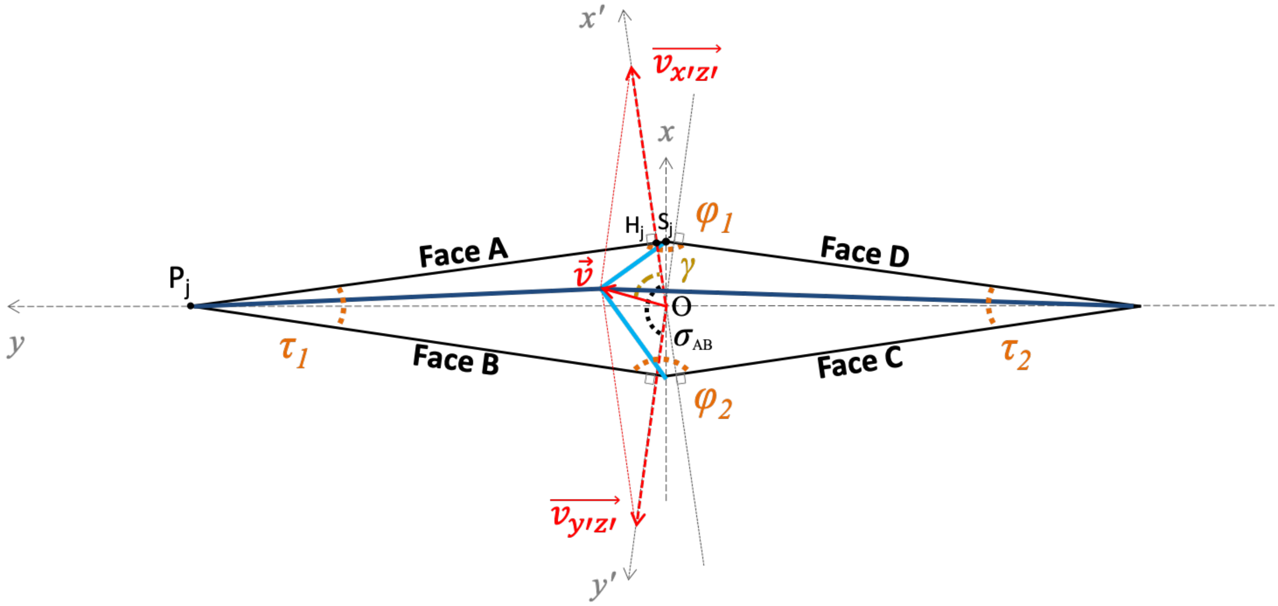

Fig. 8. Upper view of a real Knoop indenter with axis vector **v** and its projections along x'- and y'- axis.

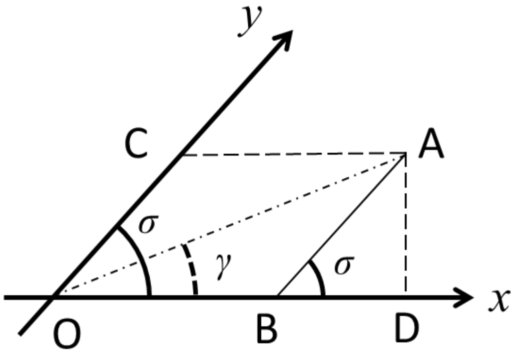

$$\begin{cases} \overline{OA}\cos\gamma = \overline{OB} + \overline{OC}\cos\sigma \\ \overline{OA}\sin\gamma = \overline{OC}\sin\sigma \end{cases}$$

Fig. 9. Generic non-orthogonal reference system with relevant equations.

$$\|\mathbf{v}\|\cos\delta = \|\mathbf{v}_{x'z'}\|\cos\delta_{\mathrm{x}'} = \left\|\mathbf{v}_{y'z'}\right\|\cos\delta_{y'} \tag{5}$$

$$\begin{aligned} &\|\mathbf{v}\|\sin\delta\cos\gamma = \|\mathbf{v}_{\mathbf{x'z'}}\|\ \sin\delta_{x'} + \left\|\mathbf{v}_{\mathbf{y'z'}}\right\|\ \sin\delta_{y'}\cos\sigma_{AB} = \\ &= \|\mathbf{v}\|\ \frac{\cos\delta}{\cos\delta_{x'}}\ \sin\delta_{x'} + \|\mathbf{v}\|\ \frac{\cos\delta}{\cos\delta_{y'}}\ \sin\delta_{y'}\cos\sigma_{AB} \end{aligned} \tag{6}$$

$$\sin\delta\cos\gamma = \frac{\cos\delta}{\cos\delta_{x'}}\sin\delta_{x'} + \frac{\cos\delta}{\cos\delta_{y'}}\sin\delta_{y'}\cos\sigma_{AB} \tag{7}$$

$$\tan\delta\cos\gamma = \tan\delta_{x'} + \tan\delta_{y'}\cos\sigma_{AB} \tag{8}$$

$$\|\mathbf{v}\|\sin\delta\sin\gamma = \|\mathbf{v}_{\mathbf{y}'\mathbf{z}'}\|\sin\delta_{y'}\sin\sigma_{AB} = \|\mathbf{v}\|\frac{\cos\delta}{\cos\delta_{y'}}\sin\delta_{y'}\sin\sigma_{AB} \tag{9}$$

$$\tan\delta\sin\gamma = \tan\delta_{y'}\sin\sigma_{AB} \tag{10}$$

By performing the squared sum of Eqs. (8) and (10), the total tilt angle δ can be obtained (see Eqs. (11)-(13)):

$$\tan^2\delta\cos^2\gamma + \tan^2\delta\sin^2\gamma = \tan^2\delta_{x'} + \tan^2\delta_{y'}\cos^2\sigma_{AB} + 2\tan\delta_{x'}\tan\delta_{y'}\cos\sigma_{AB} + \tan^2\delta_{y'}\sin^2\sigma_{AB} \tag{11}$$

$$\tan^2\delta = \tan^2\delta_{x'} + \tan^2\delta_{y'} + 2\tan\delta_{x'}\tan\delta_{y'}\cos\sigma_{AB} \tag{12}$$

$$\delta = \arctan\sqrt{\tan^2\delta_{x'} + \tan^2\delta_{y'} + 2\tan\delta_{x'}\tan\delta_{y'}\cos(\sigma_{AB})} \tag{13}$$

and from the ratio between Eqs. (10) and (8), the angle γ can be derived (see Eqs. (14)-(15)):

$$\tan\gamma = \frac{\tan\delta_{y'}\sin\sigma_{AB}}{\tan\delta_{x'} + \tan\delta_{y'}\cos\sigma_{AB}} \tag{14}$$

$$\gamma = \arctan\left(\frac{\tan\delta_{y'}\sin\sigma_{AB}}{\tan\delta_{x'} + \tan\delta_{y'}\cos\sigma_{AB}}\right) \tag{15}$$

3.2 Evaluation of the angles between the opposite edges at the vertex

From the scheme of Fig. 5 and reminding that the pyramid vertex V is placed on *z*=1, the vector of the tilted pyramid axis **v** referred to the *xyz* reference system can be written according to Eq. (16), where ρ is the mean angle between *x'*- and *x*-axis (see Eq. (2)).

$$\mathbf{v} = [\,\tan(\delta)\cos(\gamma+\rho)\,, \tan(\delta)\sin(\gamma+\rho), 1] \tag{16}$$

Considering the triangle OH$_j$V in Fig. 5 and Fig. 6 for each j-th indenter face (A, B, C, D), given that $\widehat{\mathrm{OH_jV}} = \omega_j$, and implementing the law of sines, Eq. (17) is obtained:

$$\overline{\mathrm{OH}}_j = \|\mathbf{v}\| \frac{sin\,\frac{\theta_j}{2}}{sin\,\omega_j} \tag{17}$$

where $\theta_A = \theta_C = \theta_{x'}$ and $\theta_B = \theta_D = \theta_{y'}$.

In this way, Eqs. (18) and (19) can be derived. The sign of the vector components for the four faces follows the position on the *xyz* reference system as in Fig. 5.

$$\mathbf{OS}_j = \left(\frac{\overline{\mathrm{OH}}_j}{\cos\rho_j}, 0, 0\right) \tag{18}$$

$$\mathbf{OP}_j = \left(0, \frac{\overline{\mathrm{OH}}_j}{\sin\rho_j}, 0\right) \tag{19}$$

Considering the triangle OVS$_j$, it is obtained that

$$\widehat{VOS_j} = \arccos\left(\frac{\mathbf{OS}_j \cdot \mathbf{v}}{\|\mathbf{v}\|\|\mathbf{OS}_j\|}\right) \tag{20}$$

Again, by applying the law of sines to triangle OVS$_j$, it is obtained that

$$\frac{\|\mathbf{v}\|}{\sin\widehat{OS_jV}} = \frac{\|\mathbf{OS}_j\|}{\sin\widehat{OVS_j}} = \frac{\|\mathbf{VS}_j\|}{\sin\widehat{VOS_j}} \tag{21}$$

Given that $\widehat{OS_jV} = 180 - \widehat{OVS_j} - \widehat{VOS_j}$ and with some trigonometric calculations, Eq. (22) is obtained.

$$\sin\widehat{OS_jV} = \sin\left(180 - \widehat{OVS_j} - \widehat{VOS_j}\right) = \sin\widehat{OVS_j}\cos\widehat{VOS_j} + \sin\widehat{VOS_j}\cos\widehat{OVS_j} \tag{22}$$

In this way, combining Eq. (21) and Eq.(22), Eqs. (23)-(25) are obtained:

$$\frac{\|\mathbf{v}\|}{\|\mathbf{OS}_j\|} = \frac{\sin\widehat{OS_jV}}{\sin\widehat{OVS_j}} \tag{23}$$

$$\frac{\|\mathbf{v}\|}{\|\mathbf{OS}_j\|} = \frac{\sin \widehat{OVS_j} \cos \widehat{VOS_j} + \sin \widehat{VOS_j} \cos \widehat{OVS_j}}{\sin \widehat{OVS_j}} \tag{24}$$

$$\frac{\|\mathbf{v}\|}{\|\mathbf{OS}_j\|} = \cos \widehat{VOS_j} + \frac{\sin \widehat{VOS_j}}{\tan \widehat{OVS_j}} \tag{25}$$

and from Eq. (25), Eq. (26) is also obtained:

$$\widehat{OVS_j} = \arctan\left(\frac{\|\mathbf{OS}_j\| \sin \widehat{VOS_j}}{\|\mathbf{v}\| - \|\mathbf{OS}_j\| \cos \widehat{VOS_j}}\right) \tag{26}$$

By applying the same calculations from Eq. (20) onward to triangle VOP$_j$, it is found that,

$$\widehat{OVP_j} = \arctan\left(\frac{\|\mathbf{OP}_j\| \sin \widehat{VOP_j}}{\|\mathbf{v}\| - \|\mathbf{OP}_j\| \cos \widehat{VOP_j}}\right) \tag{27}$$

Therefore, considering a single j-th indenter face, the angles between two opposite edges can be found according to:

$$\alpha_j = 2\, \widehat{OVP_j} \tag{28}$$

$$\beta_j = 2\, \widehat{OVS_j} \tag{29}$$

Averaging the results obtained for each j-th indenter face, the angles between two opposite edges, nominally 172.5° (Eq. 30) and 130° (Eq. 31), are finally obtained:

$$\alpha = \frac{\sum_{j=1}^{4} \alpha_j}{4} \tag{30}$$

$$\beta = \frac{\sum_{j=1}^{4} \beta_j}{4} \tag{31}$$

4. Comparison of experimental measurements

In order to validate the geometrical model, experimental measurements were performed on three different Knoop indenters previously verified by a German DKD accredited laboratory having comparable measurement uncertainties. Calibration certificates data with expanded uncertainties at a confidence level of 95% are reported in Table 1. Verification of the Knoop indenters' geometrical parameters was performed with the Galileo-LTF® Gal-Indent optical system at INRiM. Experimental results with expanded uncertainties at a confidence level of 95% (CMCs declared in the CIPM-MRA database) are reported in Table 2. In this way, by applying the geometrical model of Section 3, the complete set of values required for the verification of the Knoop indenters are obtained and summarized in Table 3. Expanded uncertainties (at a confidence level of 95%, *k*=2), evaluated according to GUM [26] by propagating the experimental uncertainties, are in the order of 0.05°, thus below the maximum expanded uncertainty of 0.07° required by the Standard. By way of example, the detailed uncertainty budget for the angle between the opposite edges *β* of Knoop indenter 1 is shown in Table 4.

Table 1

Calibration certificate values of the three tested Knoop indenters.

	Knoop indenter 1	*Knoop indenter 2*	*Knoop indenter 3*
ID number	3522	3528	3521
Angle between the opposite edges α /°	172.53±0.03	172.50 ± 0.03	172.50 ± 0.03
Angle between the opposite edges β /°	130.13 ± 0.07	129.83 ± 0.07	130.02 ± 0.07
Tilt angle δ /°	<0.42 ± 0.07	<0.42 ± 0.07	<0.42 ± 0.07
Numerical factor c / -	0.07018 ± 0.00030	0.07001 ± 0.00030	0.07031 ± 0.00030

Table 2

Experimental measurements on the three tested Knoop indenters.

	Knoop indenter 1	*Knoop indenter 2*	*Knoop indenter 3*
ω_A /°	25.146 ± 0.05	25.297 ± 0.05	25.197 ± 0.05
ω_B /°	25.151 ± 0.05	25.275 ± 0.05	25.184 ± 0.05
ω_C /°	25.151 ± 0.05	25.310 ± 0.05	25.193 ± 0.05
ω_D /°	25.152 ± 0.05	25.278 ± 0.05	25.174 ± 0.05
φ_1 /°	165.03 ± 0.06	163.86 ± 0.06	163.48 ± 0.06
τ_1 /°	16.07 ± 0.06	16.05 ± 0.06	15.43 ± 0.06
φ_2 /°	163.01 ± 0.06	164.23 ± 0.06	164.56 ± 0.06
τ_2 /°	15.90 ± 0.06	15.86 ± 0.06	16.53 ± 0.06

Table 3

Geometrical parameters of the three tested Knoop indenters evaluated with the geometrical model.

	Knoop indenter 1	*Knoop indenter 2*	*Knoop indenter 3*
ID number	3522	3528	3521
Angle between the opposite edges α /°	172.53 ± 0.05	172.50 ± 0.05	172.52 ± 0.05
Angle between the opposite edges β /°	130.13 ± 0.05	129.85 ± 0.05	130.06 ± 0.05
Tilt angle δ /°	0.09 ± 0.05	0.03 ± 0.05	0.06 ± 0.05
Numerical factor c / -	0.07019 ± 0.00048	0.07007 ± 0.00047	0.07019 ± 0.00048

Table 4

Unceratinty budget for the angle between the opposite edges β of Knoop indenter 1.

Variable x_k			$u^2(x_k)$	c_k	$u_k^2(a_x)$	Rank
Symbol	Value	Note				
ω_A	25.146	CMC	6,4E-04	-5,1E-01	1,7E-04	1
ω_B	25.151	CMC	6,4E-04	-5,1E-01	1,7E-04	2
ω_C	25.151	CMC	6,4E-04	-5,1E-01	1,7E-04	3
ω_D	25.152	CMC	6,4E-04	-5,1E-01	1,7E-04	4
φ_1	165.03	CMC	9,1E-04	-1,3E-02	1,5E-07	5
τ_1	16.07	CMC	9,1E-04	+1,3E-02	1,7E-07	6
φ_2	163.01	CMC	9,1E-04	-1,3E-02	1,5E-07	7
τ_2	15.90	CMC	9,1E-04	+1,3E-02	1,7E-07	8
β	130.13			Variance, $u^2(\beta)$	6,6E-04	
				St. unc. $u(\beta)$	2,6E-02	

An analysis based on the estimation of the normalized error (E_n) has been performed in order to assess the compatibility of the experimental measurements performed at INRiM with respect to calibration certificate values of the accredited laboratory, considered as reference. E_n is defined as the ratio of the difference between the measured value (x) and the reference value (y) compared to the root sum square of associated expanded uncertainties (U_x and U_y) at a confidence level of 95 % ($k = 2$). According to ISO/IEC 17043:2010 [27], it is evaluated as follows:

$$E_n = \frac{|x-y|}{\sqrt{U_x^2+U_y^2}} \tag{33}$$

Data can be considered compatible when $E_n < 1$. This is an indicator of accuracy/inaccuracy as compared to an assigned reference value with respect to the associated uncertainties.

Combining data in Table 1 and Table 3, it is found that E_n is less than 1 for all geometrical parameters as shown in Table 5. For tilt angle δ, since the calibration certificates report only that the values fall below the limit imposed by the standard, it is not possible to provide the exact normalized error. However, also experimental results show values below the standard limits. Given such evidence, the proposed method provides measurements compatible with the accredited laboratory.

Table 5

Normalized errors E_n evaluated for the three tested Knoop indenters.

	Knoop indenter 1	*Knoop indenter 2*	*Knoop indenter 3*
Angle between the opposite edges α	0.03	0.06	0.46
Angle between the opposite edges β	0.04	0.19	0.33
Numerical factor c	0.02	0.11	0.21

5. Conclusions

ISO 4545-2 and 4545-3 of Knoop hardness tests require the geometrical verification of the indenter. At present, verification of Knoop hardness is performed by few manufacturers and laboratories that use specific instrumentation for the purpose. Since the verification of Vickers indenters can be performed by a larger number of calibration laboratories and industries with dedicated systems and given the similar geometry of the two indenters, the possibility to use Vickers-addressed systems for the verification of Knoop indenters, in order to extend the measurement capability of these laboratories, is investigated. These systems are usually based on optical measurements using microscopes, scanning interferometry or confocal probes. INRiM hardness laboratory, in particular, uses a specific optical measuring system, based on Mirau interferometry, developed in cooperation with Galileo-LTF® and commercialized by Galileo-LTF® as Gal-Indent. It is able to measure the two vertex angles of the indenter between two opposite faces, the quadrilateral base angles and the angle between the axis of the diamond pyramid and the axis of the indenter holder. This paper deals with the possibility to use such quantities as inputs of a suitable geometrical model in order to verify the geometry of Knoop indenters, i.e. to evaluate the angles between the opposite edges at the vertex, nominally 172.5° and 130°, and the angle between the axis of the diamond pyramid and the axis of the indenter holder, nominally 0°. The proposed geometrical model is described in Section 3. Experimental measurements, together with the associated expanded uncertainties, were performed on three different Knoop indenters, previously measured by a

German DKD accredited laboratory, to verify the reliability of the model. Results of this work allow to highlight the following points:

- Using Vickers-addressed measured quantities as input of the proposed geometrical model allows to verify the geometry of Knoop indenters as requested by the relevant Standard.
- Comparison of measurement data with reference values shows compatible results in terms of normalized error, thus validating the proposed procedure.
- Expanded uncertainties are in the order of 0.05°, thus below the maximum expanded uncertainty of 0.07° required by the Standard.
- The advange of this geometrical model is that it can be easily implemented, even on common spreadsheets, and exploited by laboratories that adopt similar measuring systems addressed for the verification of Vickers indenters without any modification of the experimental apparatus.

References

[1] F. Knoop, C. C. Peters, W. B. Emerson, A sensitive pyramidal diamond tool for indentation measurements, Journal of Research of the National Bureau of Standards 23 (1939) 39-61.

[2] J. Borc, Study of Knoop microhardness anisotropy on the (001), (100) and (010) faces of gadolinium calcium oxyborate single crystals, Mater. Chem. Phys. 148 (2014) 680–685.

[3] F. Petik, Problems of hardness measurement, Measurement 1(1) (1983) 24–30.

[4] G. Barbato, F. Petik, Metrological involvement in the definition and dissemination of hardness scales, in: Proceedings of XIII IMEKO, vol. 1, Torino, 1994, pp. 761–766.

[5] G. Barbato, M. Galetto, A. Germak, F. Mazzoleni, Influence of the indenter shape in Rockwell hardness test, in: Proceedings of the HARDMEKO ‘98, September 21–23, Beijing, China, 1998, pp. 53–60.

[6] R.S. Marriner, J.G. Wood, Investigation into the measurement and performance of Rockwell C diamond indenters, Metallurgia 87 (1967) 87–90.

[7] G. Barbato, S. Desogus, R. Levi, The meaning of the geometry of Rockwell indenters, IMGC Tech. Rep. R128 (1978).

[8] L. Brice, The influence of indenter characteristics on hardness measurements, in: Proceedings of XVII IMEKO World Congress Metrology, Dubrovnik, Croatia, June 22-27, 2003.

[9] M. El-Sherbiny, R. Hegazy, M. Ibrahim, and A. Abuelezz, The influence of geometrical tolerances of Vickers indenter on the accuracy of measured hardness, Int. J. Metrol. Qual. Eng. 3 (2012) 1–6.

[10] A.E. Giannakopoulos, Elastic and viscoelastic indentation of flat surfaces by pyramid indentors, Journal of the Mechanics and Physics of Solids 54 (2006) 1305–1332.

[11] C. Chuenarrom, P. Benjakul, P. Daosodsai, Effect of indentation load and time on knoop and vickers microhardness tests for enamel and dentin, Materials Research 12(4) (2009) 473-476.

[12] K. Sangwal, B. Surowskab, P. Błaziak, Analysis of the indentation size effect in the microhardness measurement of some cobalt-based alloys, Materials Chemistry and Physics 77 (2002) 511–520.

[13] M. I. Simões, J. M. Antunes, J. V. Fernandes, N. A. Sakharova, Numerical simulation of the depth-sensing indentation test with Knoop indenter, Metals 8 (2018) 885.

[14] L. Riester, P.J. Blaua, E. Lara-Curzioa, K. Brederb, Nanoindentation with a Knoop indenter, Thin Solid Films 377-378 (2000) 635-639.

[15] ISO 4545:2017-2 Metallic materials — Knoop hardness test — Verification and calibration of testing machines.

[16] ISO 4545:2017-3 Metallic materials — Knoop hardness test — Calibration of reference blocks.

[17] S. Takagi, K. Kamijo, T. Usuda, H. Kawachi, K. Hanaki, Wide-range verification of the geometry of Vickers diamond indenters, in: Proceedings of XVIII IMEKO World Congress Measurement, Rio de Janeiro, Brazil, September 17-22, 2006.

[18] K. Hasche, K. Herrmann, F. Pohlenz, K. Thiele, Determination of the geometry of microhardness indenters with a scanning force microscope, Meas. Sci. Technol. 9 (1998) 1082–1086.

[19] T. Sanponpute, W. Limthunyalak, F. Menelao, D. Schwenk, Vickers indenter shape measurement by using scanning confocal chromatic instrument, in: Proceedings of XXI IMEKO World Congress “Measurement in Research and Industry”, Prague, Czech Republic, August 30 - September 4, 2015.

[20] G. Barbato, G. Gori, Metrological references in Hardness Measurement: a necessary background for industrial Quality Assurance, In: Proceedings of the 5th Congreso Nacional de Metrologia Industrial, Zaragoza, Spain, 13-15 November, 1991, pp. 139-149.

[21] G. Barbato, S. Desogus, Measurement of the spherical tip of Rockwell indenters, Journal of Testing and Evaluation 16(4) (1988) 369-374.

[22] A. Liguori, A. Germak, G. Gori, E. Messina, Galindent: the reference metrological system for the verification of the geometrical characteristics of Rockwell and Vickers diamond indenters, In: VDI/VDE-GMA, IMEKO TC3/TC5/TC20 Joint International Conference, 24-26 Sept. 2002, VDI-Berichte 1685, Tagung Celle, Germany, 2002, pp. 365-371.

[23] F.C. Campbell, Inspection of Metals: Understanding the Basics, ASM International, 2013.

[24] A. Germak, A. Liguori, C. Origlia, Experience in the metrological characterization of primary hardness standard machines, in: Proceedings of HARDMEKO 2007, Tsukuba, Japan, November 19-21, 2007, pp. 81-89.

[25] A. Prato, D. Galliani, C. Origlia, A. Germak, A correction method for Vickers indenters squareness measurement due to the tilt of the pyramid axis, Measurement 140 (2019) 565-571.

[26] JCGM 100:2008, Evaluation of Measurement Data — Guide to the Expression of Uncertainty in Measurement (GUM), Joint Committee for Guides in Metrology, Sèvres, France.

[27] ISO/IEC 17043:2010, Conformity assessment - General requirements for proficiency testing. International Organization for Standardization, Geneva, Switzerland.